4 The fundamental plane of massive quiescent galaxies out to $z \sim 2$

Abstract

The Fundamental Plane (FP) of early-type galaxies, relating the effective radius, velocity dispersion and surface brightness, has long been recognized as a unique tool for analyzing galaxy structure and evolution. With the discovery of distant quiescent galaxies and the introduction of high sensitivity near-infrared spectrographs, it is now possible to explore the FP out to $z \sim 2$. In this chapter we study the evolution of the FP out to $z \sim 2$ using kinematic measurements of massive quiescent galaxies ($M_* > 10^{11} M_\odot$). We find preliminary evidence for the existence of a FP out to $z \sim 2$. The scatter of the FP, however, increases from $z \sim 0$ to $z \sim 2$, even when taking into account the larger measurement uncertainties at higher redshift. We find a strong evolution of the zero point from $z \sim 2$ to $z \sim 0$: $\Delta \log_{10} M/L_g \propto (-0.49 \pm 0.03)\, z$. In order to assess whether our spectroscopic sample is representative of the early-type galaxy population at all redshifts, we compare their rest-frame $g - z$ colors with those from a larger mass complete sample of quiescent galaxies. At $z > 1$ we find that the spectroscopic sample is bluer. We use the color offsets to estimate a mass-to-light ratio (M/L) correction. The implied FP zero point evolution after correction is significantly smaller: $\Delta \log_{10} M/L_g \propto (-0.39 \pm 0.02)\, z$. This is consistent with an apparent formation redshift of $z_{\rm form} = 6.62^{+3.19}_{-1.44}$ for the underlying population, ignoring the effects of progenitor bias. A more complete spectroscopic sample is required at $z \sim 2$ to properly measure the M/L evolution from the FP evolution.

Jesse van de Sande, Mariska Kriek, Marijn Franx,
Rachel Bezanson, and Pieter G. van Dokkum

Revised version
Accepted for publication in the Astrophysical Journal

4.1 Introduction

The Fundamental Plane (FP) of early-type galaxies is the empirical relation between the effective radius r_e, stellar velocity dispersion within one effective radius σ_e, and the average surface brightness within one effective radius I_e (e.g., Djorgovski & Davis 1987; Dressler et al. 1987; Jorgensen et al. 1996). Traditionally, the offset in the FP is interpreted as the mass-to-light ratio (M/L) evolution of galaxies (e.g., Faber et al. 1987), under the assumption that early-type galaxies form a homologous family, and that all the evolution is caused by the change in luminosity. Holden et al. (2010) indeed suggests that this assumption is correct, finding that out to $z \sim 1$ the slope of the FP does not change. By extending M/L evolutionary studies to higher redshift, it is possible to put constraints on the formation epoch of massive galaxies.

The evolution of the M/L has been studied extensively out to $z \sim 1.3$ (e.g., van Dokkum & van der Marel 2007; Holden et al. 2010). The general consensus is that the evolution of the M/L appears to evolve as $\Delta \ln\ M/L_B \propto\ z$. With recent studies showing that the first massive, quiescent galaxies were already in place when the universe was only ∼3 Gyr old (e.g., Kriek et al. 2006; Williams et al. 2009), the question arises whether the FP already existed at this early epoch and how the M/L evolved.

With the advent of new NIR spectrographs, such as VLT-X-SHOOTER and Keck-MOSFIRE, it is now possible to obtain rest-frame optical spectra of quiescent galaxies out to $z \sim 2$. For example, in van de Sande et al. (2011; 2013) we obtained stellar kinematic measurements for five massive quiescent galaxies at $1.4 < z < 2.1$ (see also Toft et al. 2012; Belli et al. 2014b). Combined with high-resolution imaging and multi-wavelength catalogs, these recently acquired kinematic measurements enable the extension of FP studies beyond $z \sim 1.3$.

In this Chapter, we explore the existence of a FP at $z \sim 2$, and use the FP to measure the evolution of the M/L from $z \sim 2$ to the present-day for massive quiescent galaxies. In a parallel study, Bezanson et al. (2013b) presented the mass FP evolution. Throughout the chapter we assume a ΛCDM cosmology with Ω_m=0.3 $\Omega_\Lambda = 0.7$, and $H_0 = 70$ km s^{-1} Mpc^{-1}. All broadband data are given in the AB-based photometric system.

4.2 Data

For the work presented in this chapter, we use a variety of datasets, which all contain accurate kinematic measurements of individual galaxies and high quality broadband photometric catalogs. For more details see Table 4.1 and Chapter 5. All velocity dispersions presented here are aperture corrected to one effective radius following the method as described in van de Sande et al. (2013).

Stellar masses are derived using the FAST code (Kriek et al., 2009). We use the Bruzual & Charlot (2003) Stellar Population Synthesis (SPS) models and assume an exponentially declining star formation history, the Calzetti et al. (2000) dust attenuation law, and the Chabrier (2003) stellar initial mass function. For galaxies in the SDSS, stellar masses are from the MPA-JHU DR7[1] release which are based on Brinchmann et al. (2004).

[1] http://www.mpa-garching.mpg.de/SDSS/DR7/

Table 4.1: Data references sample

Survey & Field	N_{gal}	z	Spectroscopy	Telescope & Instrument	Photometric Catalog	Structural Parameters
SDSS DR7	4621	$0.05 < z < 0.07$	Abazajian et al. (2009)	SDSS	Blanton et al. (2005)	Simard et al. (2011)
NMBS-COSMOS	3	$0.7 < z < 0.9$	Bezanson et al. (2013b)	Keck-DEIMOS	Skelton et al. (2014)	Bezanson et al. (2011)
	10				Whitaker et al. (2011)	
UKIDSS-UDS	3	$0.6 < z < 0.7$	Bezanson et al. (2013b)	Keck-DEIMOS	Skelton et al. (2014)	van der Wel et al. (2012)
	1				Williams et al. (2009)	
MS 1054-0321	8	$z = 0.83$	Wuyts et al. (2004)	Keck-LRIS	Förster Schreiber et al. 2006	Blakeslee et al. (2006)
GOODS-S	7	$0.9 < z < 1.2$	van der Wel et al. (2005)	VLT-FORS2	Skelton et al. (2014)	van der Wel et al. (2012)
GOODS-N	1	$z = 1.315$	Newman et al. (2010)	Keck-LRIS	Skelton et al. (2014)	van der Wel et al. (2012)
EGS	8	$1.0 < z < 1.3$	Belli et al. (2014a)	Keck-LRIS	Skelton et al. (2014)	van der Wel et al. (2012)
COSMOS	6	$1.1 < z < 1.3$	Belli et al. (2014a)	Keck-LRIS	Skelton et al. (2014)	van der Wel et al. (2012)
GOODS-S	1	$z = 1.419$	Belli et al. (2014a)	Keck-LRIS	Skelton et al. (2014)	van der Wel et al. (2012)
NMBS-COSMOS	4	$1.2 < z < 1.5$	Bezanson et al. (2013a)	Keck-LRIS	Whitaker et al. (2011)	Bezanson et al. (2013a)
NMBS-AEGIS	2	$1.4 < z < 1.6$	Bezanson et al. (2013a)	Keck-LRIS	Whitaker et al. (2011)	Bezanson et al. (2013a)
NMBS-COSMOS	2	$1.6 < z < 2.1$	van de Sande et al. (2013)	VLT-XShooter	Skelton et al. (2014)	van de Sande et al. (2013)
	1				Whitaker et al. (2011)	
UKIDSS-UDS	1	$1.4 < z < 2.1$	van de Sande et al. (2013)	VLT-XShooter	Skelton et al. (2014)	van de Sande et al. (2013)
	1				Williams et al. (2009)	
COSMOS	1	$z = 1.823$	Onodera et al. (2012)	Subaru-MOIRCS	Muzzin et al. (2013a)	Onodera et al. (2012)
MUSYC 1255	1	$z = 2.286$	van Dokkum et al. (2009)	Gemini-GNIRS	Blanc et al. (2008)	van Dokkum et al. (2009)
COSMOS	2	$2.1 < z < 2.3$	Belli et al. (2014b)	Keck-MOSFIRE	Skelton et al. (2014)	Belli et al. (2014b)

The photometry and thus also the stellar mass are corrected for missing flux using the best-fit Sérsic luminosity (Taylor et al., 2010). Effective radii and other structural parameters, such as Sérsic index and axis ratio, are determined using 2D-Sérsic fits with GALFIT (Peng et al., 2010). The effective radii are circularized, i.e., $r_{\rm e} = \sqrt{ab}$. All rest-frame fluxes, including those for the SDSS sample, are calculated using the photometric redshift code EAZY (v46; Brammer et al. 2008).

We derive the average surface brightness within one $r_{\rm e}$ ($I_{\rm e}$, in units of $L_{\odot,{\rm g}}$ pc^{-2}) by dividing the total luminosity in the rest-frame g-band by $2\pi r_{\rm e}^2$. Absolute g-band magnitudes are calculated with $M_{\odot,{\rm g}} = 5.14$, which we derive from the solar spectrum taken from the CALSPEC database[2].

We adopt a mass limit ($M_* > 10^{11}\ M_\odot$) to homogenize the final sample. We note, however, that our sample remains relatively heterogeneous and in particular the higher redshift samples are biased toward the brightest galaxies (see also Section 4.4). We furthermore use the $U-V$ vs. $V-J$ rest-frame color selection criteria to remove star-forming galaxies from our sample (e.g., Wuyts et al. 2007; Williams et al. 2009). Quiescent galaxies are selected to have $U-V > (V-J)\times 0.88 + 0.59$. This criteria is slightly different from previous work, as we do not require that $U-V > 1.3$ or $V-J < 1.5$. The latter criteria removes post-starburst galaxies and very old galaxies, respectively.

4.3 The fundamental plane

The FP is traditionally written as:

$$\log_{10} r_{\rm e} = a \log_{10} \sigma_{\rm e} + b \log_{10} I_{\rm e,g} + c_{\rm r} \tag{4.1}$$

with $r_{\rm e}$ in kpc, $\sigma_{\rm e}$ in km s^{-1}, and $I_{\rm e,g}$ in $L_{\odot,{\rm g}}$ pc^{-2}. In this chapter, we adopt the slope from Jorgensen et al. (1996), i.e., $a = 1.20$, and $b = -0.83$. While detailed studies on galaxies in the SDSS have shown that the slope is steeper, i.e., $a = 1.404$, and $b = -0.76$ (Hyde & Bernardi, 2009), we nonetheless adopt the Jorgensen et al. (1996) values, for an easier comparison with previous high-redshift studies. We do not fit the slope ourselves at high redshift, as our sample is too small and biased at $z > 1$. However, we note that Holden et al. (2010) find the same slope of the FP at $z \sim 1$ as Jorgensen et al. (1996).

While the projection of the FP along the effective radius is most often shown, the projection along $\log_{10} I_{\rm e}$ directly shows the evolution in the M/L, which is thought to be the main driver in the evolution of the FP zero point. The top row in Figure 4.1 shows the following projection:

$$\log_{10} I_{\rm e} = a \log_{10} \sigma_{\rm e} + b \log_{10} r_{\rm e} + c_{\rm I}, \tag{4.2}$$

with $a = 1.45$, $b = -1.20$, and $c_{\rm I} = -0.11$. We determine the zero point $c_{\rm I}$ using a least-square fit, using the IDL function $MPFIT$ (Markwardt, 2009). The zero point evolves rapidly with redshift: $0.30,\ 0.54,\ 0.96$ dex, at $z \sim 0.75,\ z \sim 1.25,\ z \sim 2.00$, respectively.

[2] http://www.stsci.edu/hst/observatory/cdbs/calspec.html

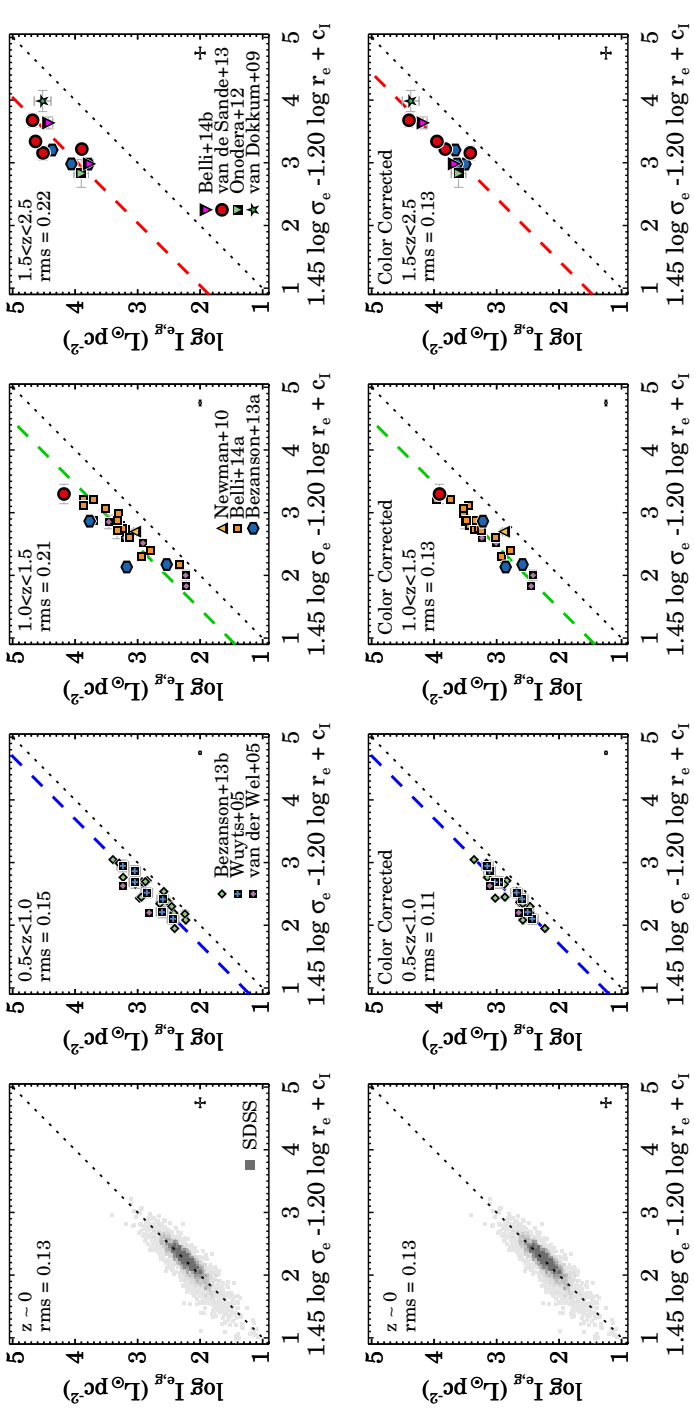

Figure 4.1: Edge on projections of the FP of massive quiescent galaxies ($M_* > 10^{11} M_\odot$) from low to high redshift. Top: at $z > 0.5$ galaxies no longer fall on the SDSS FP (dotted line), with the dashed line indicating the best-fit relation. The rms scatter increases from $z \sim 0 - z \sim 2$, and cannot be explained by larger measurement errors at $z > 1$ alone. Bottom: Similar as top row, but now including a color correction applied to all galaxies in our spectroscopic sample, to fix the sample bias toward bright young galaxies (see Section 4.4). With the correction applied, we find that the scatter around the FP now reduces for the three high-redshift bins, implying that a tight FP exists out to $z \sim 2$.

The top row in Figure 4.1 suggests that the FP exist out to $z \sim 2$. However, to quantify the existence of a FP, we consider the scatter before and after the FP fit, i.e., the rms scatter in $\log_{10} I_e$ vs. the scatter in $(a \log_{10} \sigma_e + b \log_{10} r_e) - \log_{10} I_e$ or $\Delta \log_{10} I_e$.

For example, for galaxies in the SDSS for which we know the FP exists, the scatter in $\log_{10} I_e$ is 0.26 ± 0.003 dex before the fit, while after the fit, we measure $\Delta \log_{10} I_e = 0.13 \pm 0.002$ dex. At $z = 2$ we find a decrease as well, from $\log_{10} I_e = 0.33 \pm 0.04$ dex, before the fit, to $\Delta \log_{10} I_e = 0.25 \pm 0.04$ after the fit. This hints to the existence of a FP at $z \sim 2$, although the scatter in dex is almost twice as high compared to $z \sim 0$.

We use Monte-Carlo simulations to determine if the scatter could be due to measurement uncertainties alone. We find that scatter induced by observational errors is 0.14 dex at $z \sim 2$, resulting in an intrinsic scatter of 0.20 dex. Compared to the FP scatter at $z \sim 0$, the intrinsic scatter at $z \sim 2$ is still higher. The larger scatter could have been caused by the large range in age and the bias toward post-starburst galaxies.

4.4 Correcting for sample bias

In order to explain the larger scatter in the FP of our high-redshift sample, we compare the rest-frame $g-z$ colors of our spectroscopic sample to a larger photometric and more complete galaxy sample. We use galaxies from the 3D-HST survey (v4.1; Brammer et al. 2012; Skelton et al. 2014), which were selected to be massive ($M_* > 10^{11} M_\odot$), non-star-forming according to their $U-V$ vs. $V-J$ colors (see Section 4.2), and have a reduced $\chi^2 < 5$ for the best-fit stellar population model to their SED. Rest-frame fluxes for the reference sample were derived with EAZY, in a similar fashion as for the spectroscopic sample and are based on photometric redshifts.

In Figure 4.2(a) we show the comparison of the rest-frame $g - z$ color as a function of redshift. The reference sample is binned in redshift, with the median of each bin shown as a big gray circle. The dashed line shows the best fit of the color as a function of redshift: $(g-z)_{\rm rf} = -0.16z + 1.49$. There is very little difference between the reference and the spectroscopic sample at $0 < z < 1$, while at $z > 1$ the spectroscopic sample becomes increasingly bluer compared to the median of the reference sample. At $z > 1.4$ we furthermore see a large spread in colors, where some galaxies follow the median of galaxy the population, while other galaxies are offset by more than 0.5 mag.

All spectroscopic samples are relatively blue at higher redshift, as it is easier to obtain high signal-to-noise spectra for quiescent galaxies compared to the much fainter older quiescent galaxies. In order to estimate the effect of this bias, we use the color difference with the reference sample to calculate a M/L correction for the individual galaxies in our spectroscopic sample.

First, we measure the relative evolution of the M/L from the FP as shown in the top panels of Figure 4.1, under the assumption that a, and b do not evolve with redshift:

$$\Delta \log_{10} M/L = c_z - c_0. \tag{4.3}$$

Here c_0 is the FP zeropoint at redshift zero, while c_z is determined from the residuals from the FP for each individual galaxy at redshift z :

$$c_z = (a \log_{10} \sigma_e + b \log_{10} r_e) - \log_{10} I_e \tag{4.4}$$

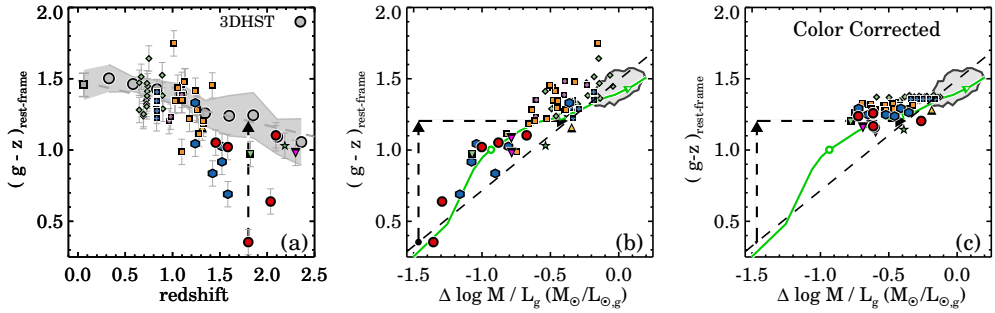

Figure 4.2: Redshift evolution of rest-frame $g-z$ color and M/L correction from color offset. (a) $(g-z)_{\rm rest-frame}$ colors for our high-redshift spectroscopic sample compared to a larger and more complete photometric sample from the 3DHST survey with a similar mass selection as shown by the large gray circles. The gray area indicates the $1-\sigma$ scatter. For the reference sample we measure that $(g-z)_{\rm rest-frame}$ evolves as $-0.16z$ (dashed gray line). At $z>1$ the spectroscopic sample becomes increasingly bluer than the reference sample, indicating a rather strong selection bias. (b) $\log_{10} M/L_g$ vs. rest-frame $g-z$ color. Massive galaxies from the SDSS are shown by the gray contour, which encloses 68% of all galaxies. The green line shows a Ma11 model, and the dashed black line shows the linear approximation to the model ($\log_{10} M/L \propto 1.29(g-z)_{\rm rest-frame}$). We use the model approximation to correct the M/L using the color offset. The correction is demonstrated with the arrows for the galaxy with the lowest M/L and bluest color. (c) Corrected M/Ls and $g-z$ colors. The correction is small for most low-redshift galaxies (~ 0.2 dex), while the galaxies at $z>1.5$ have larger corrections of $\sim 0.2-1.0$ dex.

Note that we have $\Delta \log_{10} M/L = \Delta \log_{10} I_e$.

Next, we use the relation between the rest-frame $g-z$ color and the derived $\Delta \log_{10} M/L$ as shown in Figure 4.2(b) to derive the M/L correction. There is a correlation between the color and M/L, where the bluest galaxies have the lowest M/L. This correlation is also predicted by SPS models, on which we base our M/L correction. In Figure 4.2(b) we show a Maraston & Strömbäck (2011, Ma11) solar metallicity model (green line), with a truncated star formation history and constant star formation for the first 0.5-Gyr. Different ages in this model are indicated on the green line by the circle (0.3-Gyr), diamond (1.0-Gyr), and triangle (10-Gyr). We approximate the Ma11 model by a simple linear fit: $\log_{10} M/L \propto 1.29(g-z)_{\rm rf}$ (dashed black line). We use this fit to estimate the M/L correction.

As an example, we highlight the bluest galaxy in our sample, NMBS-Cos-7447 at $z\sim 1.8$. In Figure 4.2(a), the black arrow indicates the color offset to the $(g-z)_{\rm rest-frame}$ color-redshift relation. The same galaxy has an extremely low M/L as is clear from Figure 4.2(b). Here the vertical arrow is again the color offset of this galaxy, but the horizontal arrow now points toward the M/L that the galaxy would have, if it would fall on the color-redshift relation from Figure 4.2(a). The M/L correction that we apply to this individual galaxy is therefore the length of the horizontal arrow. In other words, for each galaxy we lower the M/L by 1.29 times the color offset, where the factor 1.29 comes from the linear fit to the Ma11 model (dashed line). We note, however, that a steeper M/L vs. color relation yields larger M/L corrections, and thus impacts the M/L evolution in Section 4.5. We show the corrected colors and M/L for the entire sample in Figure 4.2(c). The rest-frame $g-z$ color and M/L of the spectroscopic sample is now similar to that of the reference sample.

With the M/L (or $\Delta \log_{10} I_e$) correction applied, we can return to the FP which is shown in the bottom row of Figure 4.1. As before, the dashed colored lines indicate the best-fit FP

with the following zero points in each redshift bin: 0.30, 0.53, and 0.62 dex, from low to high redshift. Note that the $z \sim 2$ zero point is significantly lower than before the correction. The scatter around the FP is greatly reduced for all three redshift bins. In particular for the highest redshift bin, which had the largest spread in $(g-z)_{\rm rf}$ color, the scatter has decreased by almost a factor two. More quantitatively, the scatter after the FP fit is: $\Delta \log_{10} I_{\rm e} = 0.11 \pm 0.02,\ 0.13 \pm 0.02,\ 0.14 \pm 0.02$, from low to high redshift, respectively. We note that the small scatter is most likely a lower limit, as we do not include the intrinsic color scatter in our analysis.

4.5 Evolution of the M/L

In Figure 4.3 we show the M/L as derived from the FP offset relative to $z \sim 0$, as a function of redshift for all galaxies. We indicate the different zero points from Figure 4.1 as dashed lines. The red solid line is a linear least-square fit to all data, which describes the evolution of the M/L : $\Delta \log_{10} M/L_{\rm g} \propto (-0.49 \pm 0.03)\ z$. Here we have anchored the fit to the median of the $z \sim 0$ SDSS galaxies. When excluding SDSS from the fit, the evolution is more rapid: $\Delta \log_{10} M/L_{\rm g} \propto (-0.61 \pm 0.09)\ z$.

The evolution is similar to a previous result by van Dokkum & van der Marel (2007), who find that the $M/L \propto (-0.555 \pm 0.042)\ z$ in the rest-frame B-band. Here, the effect of using a slightly bluer rest-frame filter makes very little difference, i.e., our measured M/L evolution in the rest-frame B-band is only slightly faster as compared to the g-band: $\Delta \log_{10} M/L_{\rm B} \propto (-0.53 \pm 0.03)\ z$.

For a fair comparison with previous studies, we also restrict the fit to $z < 1.4$, and find a slower evolution than other studies: $\Delta \log_{10} M/L_{\rm g} \propto (-0.45 \pm 0.01)\ z$. This suggest that the relatively fast evolution of the entire sample is mainly driven by galaxies at $z > 1.4$. This is furthermore evident from Figure 4.3(a) in which almost all $z > 1.4$ galaxies fall below the best fit for the entire sample.

Figure 4.3(b) shows the M/L evolution with redshift, with the M/L correction included. This time, we find a milder evolution in the M/L than before: $\Delta \log_{10} M/L_{\rm g} \propto (-0.39 \pm 0.02)\ z$, shown by the red line. Our corrected M/L evolution is similar to previous studies by e.g., van Dokkum & Stanford (2003) (-0.460 ± 0.039), and Holden et al. (2005) (-0.426 ± 0.04), but slower than the evolution found by van Dokkum & van der Marel (2007) (-0.555 ± 0.04), and Holden et al. (2010) (-0.60 ± 0.04). If we would have used a steeper M/L vs. color relation for the correction, (e.g., $\log_{10} M/L \propto\ 1.80(g-z)_{\rm rest-frame}$) the M/L evolution would be slower: $\Delta \log_{10} M/L_{\rm g} \propto (-0.36 \pm 0.03)\ z$.

We also show the single burst Ma11 model from Figure 4.2, with a formation redshift of infinity. Using the same Ma11 model, we fit the average formation redshift of the biased sample (Figure 4.3(a)), and estimate $z_{\rm form} = 3.29^{+0.55}_{-0.56}$. For our corrected sample (Figure 4.3(b)) we estimate the apparent $z_{\rm form} = 6.62^{+3.19}_{-1.44}$. The large difference highlights the strong selection bias in the sample. Both estimates ignore the progenitor bias, which is very strong given the fact that the number density of massive galaxies changes by a factor of ~ 10 from z $\sim$ 2 to z $\sim$ 0 (Muzzin et al., 2013b).Therefore, the corrected $z_{\rm form}$ should be regarded as an upper limit for a mass-complete sample that is not supplemented by newly quenched galaxies at later times. We note that we would find a lower $z_{\rm form}$ if we were to include progenitor bias in our

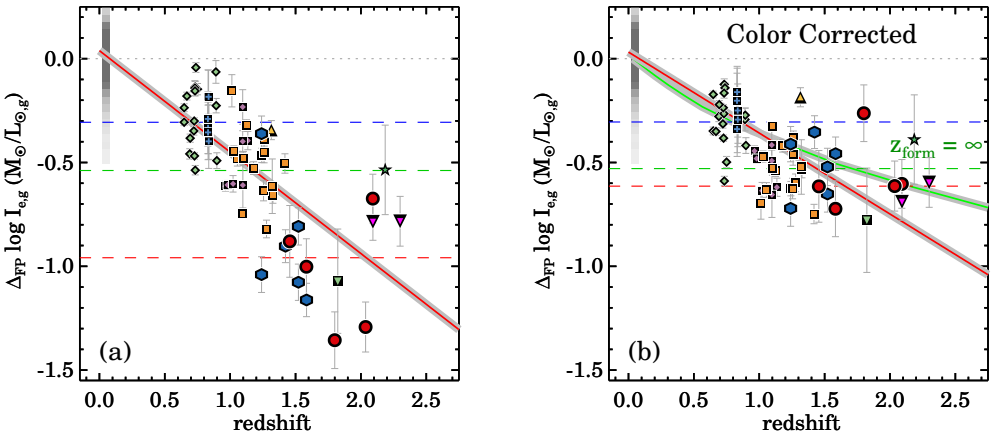

Figure 4.3: (a) Redshift evolution of the residuals from the FP. We show the residual from the FP, $\Delta \log_{10} I_{e,g}$ vs. redshift as compared to $z \sim 0$, with the dashed colored lines corresponding to the best-fit offset for the different redshift regimes indicated in Figure 4.1. The red line shows the best fit described by $\Delta \log_{10} M/L \propto -0.49z \pm 0.03$, where we have anchored the fit to the median of the SDSS data. We find a similar evolution of the M/L as compared to previous work, while the high-redshift data at $z > 1.25$ have lower M/L. (b) Similar to (a), but now including a correction based on the offset from the $(g-z)_{\rm rest-frame}$ relation. This time, we find a milder evolution of $\Delta \log_{10} M/L_g \propto (-0.39 \pm 0.02)\ z$ indicated by the red line, while we show the uncorrected evolution as the dashed gray line. We also include a single burst Ma11 model, with solar metallicity, and with $z_{\rm form} = \infty$ (green line).

analysis, or if we would use an evolving mass limit in our sample-selection. A more detailed study of this effect would require a mass-complete spectroscopic sample.

4.6 Discussion

In Section 4.4 we have corrected our sample for the bias toward young quiescent galaxies. In this correction we assume that all quiescent galaxies at a particular redshift have the same color and thus the same age. This assumption is an oversimplification, and the scatter in the FP is actually partly due to age variations (e.g., Graves et al. 2009). Furthermore, the age variations of quiescent galaxies may increase with redshift, as shown by Whitaker et al. (2010). Thus, it is very likely that the scatter in the FP will be induced by larger age variations at higher redshift.

However, as we apply the same correction at all redshifts, we do show that the scatter in the FP due to variation in other properties than age (e.g., evolution in stellar mass, size, velocity dispersion, and metallicity) is approximately constant over time. Though, our M/L evolution is not necessarily the M/L evolution of progenitors and descendants of a fixed population, as the masses, sizes, and velocity dispersions of these galaxies likely evolve systematically with redshift. Using a simple model, we can estimate the effect of structural evolution on the FP and M/L evolution. Given that mass evolves as $\Delta \log_{10} M/M_\odot \sim 0.15z$ (van Dokkum et al., 2010), we found that $\Delta\, r_e \propto M^{1.83} \simeq M^2$, and $\Delta\, \sigma_e \propto M^{-0.49} \simeq M^{-0.5}$ in van de Sande et al. (2013). Thus, if mass grows by a factor f, the M/L evolution (from Equations

4.3&4.4) including structural evolution can be written as follows:

$$\Delta \log_{10} M/L \simeq \; a \log_{10}(f^{-0.5}\sigma_{\rm e}) + b \log_{10}(f^{2} r_{\rm e}) - \log_{10}(f^{-3} I_{\rm e}) \qquad (4.5)$$

The bias in the M/L evolution induced by structural evolution can therefore be approximated by $(-0.5a + 2b + 3) \log_{10} f$. Assuming a mass growth factor of 0.3 dex, we find that the offset in the M/L due to structural evolution is small: ~ 0.04 dex. We note that if velocity dispersion does not evolve, this effect is larger: ~ 0.2 dex.

4.7 Conclusion

In this chapter, we have used stellar kinematic and structural measurements of massive quiescent galaxies ($M_* > 10^{11} M_\odot$) out to $z \sim 2$ to the study the evolution of the rest-frame g-band fundamental plane. We utilize this empirical relation between the size, stellar velocity dispersion, and the surface brightness, to constrain the evolution of the M/L.

We find preliminary evidence for the existence of a FP out to $z \sim 2$, but with larger scatter as compared to the present-day FP for massive quiescent galaxies from the SDSS. There is a rapid evolution of the FP zero point from $z \sim 0$ to $z \sim 2 : \Delta \log_{10} M/L_{\rm g} \propto (-0.49 \pm 0.03)\, z$. Furthermore, we find that the $M/L_{\rm g}$ evolution for galaxies at $z > 1.4$ is faster than for galaxies at $z < 1.4$.

The larger scatter and fast evolution can be explained by the fact that our spectroscopic sample becomes increasingly bluer at high redshift compared to a mass complete sample of quiescent galaxies. We calculate the color difference between the galaxies and the mass complete sample, and estimate the systematic effect on the M/L.

With this correction applied, the evolution of the M/L, as derived from the FP, is slower: $\Delta \log_{10} M/L_{\rm g} \propto (-0.39 \pm 0.02)\, z$. A simple model, ignoring progenitor bias, would imply a formation redshift of $z_{\rm form} = 6.62^{+3.19}_{-1.44}$ for a mass complete sample. The difference between the evolution of our observed sample and the underlying population, highlights the need for a more detailed study of a mass complete spectroscopic sample.

Acknowledgments

We thank the NMBS and 3DHST collaborations, Rik Williams, Ryan Quadri, and Andrew Newman for providing ancillary data. This work is based on observations taken by the 3D-HST Treasury Program (GO-12177,12328) with the NASA/ESA-HST, which is operated by the Association of Universities for Research in Astronomy, Inc., under NASA contract NAS5-26555.

References

Abazajian, K. N., Adelman-McCarthy, J. K., Agüeros, M. A., et al. 2009, ApJS, 182, 543
Belli, S., Newman, A. B., Ellis, R. S., & Konidaris, N. P. 2014b, ApJ, 788, L29
Belli, S., Newman, A. B., & Ellis, R. S. 2014a, ApJ, 783, 117
Bezanson, R., van Dokkum, P., van de Sande, J., Franx, M., & Kriek, M. 2013a, ApJ, 764, L8
Bezanson, R., van Dokkum, P. G., van de Sande, J., et al. 2013b, ApJ, 779, L21
Bezanson, R., van Dokkum, P. G., Franx, M., et al. 2011, ApJ, 737, L31
Blakeslee, J. P., Holden, B. P., Franx, M., et al. 2006, ApJ, 644, 30
Blanc, G. A., Lira, P., Barrientos, L. F., et al. 2008, ApJ, 681, 1099
Blanton, M. R., Schlegel, D. J., Strauss, M. A., et al. 2005, AJ, 129, 2562
Brammer, G. B., van Dokkum, P. G., & Coppi, P. 2008, ApJ, 686, 1503
Brammer, G. B., van Dokkum, P. G., Franx, M., et al. 2012, ApJS, 200, 13
Brinchmann, J., Charlot, S., White, S. D. M., et al. 2004, MNRAS, 351, 1151
Bruzual, G., & Charlot, S. 2003, MNRAS, 344, 1000
Calzetti, D., Armus, L., Bohlin, R. C., et al. 2000, ApJ, 533, 682
Chabrier, G. 2003, PASP, 115, 763
Djorgovski, S., & Davis, M. 1987, ApJ, 313, 59
Dressler, A., Faber, S. M., Burstein, D., et al. 1987, ApJ, 313, L37
Faber, S. M., Dressler, A., Davies, R. L., Burstein, D., & Lynden-Bell, D. 1987, Nearly Normal Galaxies. From the Planck Time to the Present, 175
Förster Schreiber, N. M., Franx, M., Labbé, I., et al. 2006, AJ, 131, 1891
Graves, G. J., Faber, S. M., & Schiavon, R. P. 2009, ApJ, 698, 1590
Holden, B. P., van der Wel, A., Franx, M., et al. 2005, ApJ, 620, L83
Holden, B. P., van der Wel, A., Kelson, D. D., Franx, M., & Illingworth, G. D. 2010, ApJ, 724, 714
Hyde, J. B., & Bernardi, M. 2009, MNRAS, 396, 1171
Jorgensen, I., Franx, M., & Kjaergaard, P. 1996, MNRAS, 280, 167
Kriek, M., van Dokkum, P. G., Labbé, I., et al. 2009, ApJ, 700, 221
Kriek, M., van Dokkum, P. G., Franx, M., et al. 2006, ApJ, 649, L71
Maraston, C., & Strömbäck, G. 2011, MNRAS, 418, 2785
Markwardt, C. B. 2009, Astronomical Data Analysis Software and Systems XVIII, 411, 251
Muzzin, A., Marchesini, D., Stefanon, M., et al. 2013a, ApJS, 206, 8
Muzzin, A., Marchesini, D., Stefanon, M., et al. 2013b, ApJ, 777, 18
Newman, A. B., Ellis, R. S., Treu, T., & Bundy, K. 2010, ApJ, 717, L103
Onodera, M., Renzini, A., Carollo, M., et al. 2012, ApJ, 755, 26
Peng, C. Y., Ho, L. C., Impey, C. D., & Rix, H.-W. 2010, AJ, 139, 2097
Simard, L., Mendel, J. T., Patton, D. R., Ellison, S. L., & McConnachie, A. W. 2011, ApJS, 196, 11
Skelton, R. E., Whitaker, K. E., Momcheva, I. G., et al. 2014, arXiv:1403.3689
Taylor, E. N., Franx, M., Brinchmann, J., van der Wel, A., & van Dokkum, P. G. 2010, ApJ, 722, 1
Toft, S., Gallazzi, A., Zirm, A., et al. 2012, ApJ, 754, 3
van de Sande, J., Kriek, M., Franx, M., et al. 2013, ApJ, 771, 85
van de Sande, J., Kriek, M., Franx, M., et al. 2011, ApJ, 736, L9
van der Wel, A., Bell, E. F., Häussler, B., et al. 2012, ApJS, 203, 24
van der Wel, A., Franx, M., van Dokkum, P. G., et al. 2005, ApJ, 631, 145
van Dokkum, P. G., Whitaker, K. E., Brammer, G., et al. 2010, ApJ, 709, 1018
van Dokkum, P. G., Kriek, M., & Franx, M. 2009, Nature, 460, 717
van Dokkum, P. G., & van der Marel, R. P. 2007, ApJ, 655, 30
van Dokkum, P. G., & Stanford, S. A. 2003, ApJ, 585, 78
Whitaker, K. E., Labbé, I., van Dokkum, P. G., et al. 2011, ApJ, 735, 86
Whitaker, K. E., van Dokkum, P. G., Brammer, G., et al. 2010, ApJ, 719, 1715
Williams, R. J., Quadri, R. F., Franx, M., van Dokkum, P., & Labbé, I. 2009, ApJ, 691, 1879
Wuyts, S., van Dokkum, P. G., Kelson, D. D., Franx, M., & Illingworth, G. D. 2004, ApJ, 605, 677
Wuyts, S., Labbé, I., Franx, M., et al. 2007, ApJ, 655, 51